

# Gravitational waves from colliding vacuum bubbles in gauge theories

Marek Lewicki<sup>1,\*</sup> and Ville Vaskonen<sup>2,†</sup>

<sup>1</sup>*Faculty of Physics, University of Warsaw ul. Pasteura 5, 02-093 Warsaw, Poland*

<sup>2</sup>*Institut de Fisica d'Altes Energies (IFAE), The Barcelona Institute of Science and Technology, Campus UAB, 08193 Bellaterra (Barcelona), Spain*

We study production of gravitational waves (GWs) in strongly supercooled cosmological phase transitions, considering classically conformal scalar electrodynamics as a benchmark model. We perform lattice simulations in order to study the evolution of the complex scalar field and the gauge field in two-bubble collisions. From these simulations we extract the scaling of the GW source in the collision, which we then use in many-bubble simulations in the thin-wall limit to calculate the resulting GW spectrum. We find that in presence of the gauge field the field gradients sourcing GWs decay with the bubble size as  $\propto R^{-3}$  similarly to the real scalar case. This leads to a GW spectrum that follows  $\Omega_{\text{GW}} \propto \omega^{2.3}$  at low frequencies and  $\Omega_{\text{GW}} \propto \omega^{-2.9}$  at high frequencies. We also explore the spectra resulting for different decay laws finding that the envelope result predicting  $\omega^{-1}$  behaviour at high frequencies does not provide an accurate description of the spectrum in realistic models.

## I. INTRODUCTION

We are currently witnessing the dawn of a new era in astrophysics and cosmology, started by the LIGO/Virgo observations of gravitational waves (GWs) from black hole mergers [1, 2]. Many experiments have been planned to further explore GWs in a broader range of frequencies and with more accuracy in the coming decades [3–10]. In addition to transient GW signals, such as those from black hole mergers, these experiments are able to probe stochastic GW backgrounds. In fact, recent results from NANOGrav pulsar timing observations [11] may already indicate the first observation of a stochastic GW background (for possible interpretations see e.g. Refs. [12–21]).

Observations of stochastic GW backgrounds could allow us a glimpse of the very early Universe as many high-energy processes are predicted to be potential sources of such backgrounds. In this paper we will focus on cosmological first-order phase transitions which are one example of such a source [22]. Many beyond Standard Model scenarios predict first-order phase transitions and a significant amount of work has already been put into the possibility of exploring them through GWs [23–68].

In a first-order phase transition the Universe starts in a metastable false vacuum. The transition proceeds via nucleation and subsequent expansion of bubbles of true vacuum [69–71]. Eventually these bubbles collide and convert the whole Hubble volume into the new phase. In this process GWs are sourced by the bubble collisions [72–77] and plasma motions generated by the interactions of the plasma with the bubble walls [78–84]. In strongly supercooled transitions the former one dominates [74, 85].

For the calculation of the GWs from colliding vacuum bubbles the equations of motion of the fields sourcing

GWs need to be solved. This in principle requires 3D lattice simulations [73, 76, 86]. These simulations are computationally very expensive as very large simulation volumes are needed in order to simulate multiple bubbles and the lattice has to be very dense in order to resolve the thinning bubble walls. Therefore it is practical to develop approximations that provide a realistic description of the phase transition dynamics and an accurate estimate of the resulting GW spectrum, but are computationally less expensive than full 3D lattice simulations.

For a long time the envelope approximation, introduced in Ref. [72] and studied further in Refs. [87–89], has been used to estimate the GW spectrum sourced by the bubble collisions. In this approximation the collided parts of the bubble walls are completely neglected and the GW spectrum is calculated in the thin-wall limit. Improved modeling was developed [90–93] as an attempt to model the behaviour of the plasma after the transition. Following a similar approach in Ref. [77] we developed a new estimate for the GW spectrum from bubble collisions by accounting for the scaling of the scalar field gradients, that source GWs, after the collisions. We found significant differences as compared to the result from the envelope approximation. In particular, in our approximation the high-frequency tail of the GW spectrum is much steeper than in the envelope approximation.

In this paper we consider effective potentials of realistic models in which bubble collisions can give the dominant contribution to the GW production. Furthermore, we describe breaking of a gauge U(1) symmetry, and study with lattice simulations the evolution of the scalar field and gauge field in two-bubble collisions. We find that if  $\tilde{g} = gv^2/\sqrt{\Delta V} \gg 1$ , where  $g$  is the gauge coupling,  $v$  is the vacuum expectation value of the scalar field, and  $\Delta V$  is the vacuum energy difference between the symmetric and broken minima, the gradients in the complex phase of the scalar field are quickly damped after the collision by the gauge field. Therefore, in this limit the GW source after the collision scales in the same way independently of what the complex phase difference between the colliding

\* [marek.lewicki@fuw.edu.pl](mailto:marek.lewicki@fuw.edu.pl)

† [vvaskonen@ifae.es](mailto:vvaskonen@ifae.es)

bubbles was, and we find that the GW spectrum is  $\propto \omega^{2.3}$  at low frequencies. This is the case in most of the relevant part of the parameter space of interest. In the opposite limit,  $\tilde{g} \ll 1$ , the GW spectrum instead scales as  $\propto \omega$  at low frequencies, similarly as in the U(1) symmetric case without a gauge field, studied in Ref. [77]. At high frequencies we find in both cases that the spectrum is much steeper than in the envelope approximation.

## II. PHASE TRANSITION

In order for the bubble collisions to give the dominant GW source, the phase transition has to be strongly supercooled [74, 85]. Such strong supercooling is not typically realized in models where the scalar field potential is polynomial [74, 82]. Instead, in models featuring classical scale invariance [27, 36, 38, 40, 44, 50, 52, 60, 61, 94–102] the transition can be so strongly supercooled that the interactions of the bubble wall with the plasma can be neglected [74, 85]. Many realistic models also include a gauge U(1) symmetry under which the scalar field is charged, and the dominant contribution on the effective potential arises from the gauge field loops. The phase transition in these models is therefore similar to that in classically conformal scalar electrodynamics, which we choose as a benchmark model.

Scalar electrodynamics is described by the gauge U(1) symmetric Lagrangian

$$\mathcal{L} = -\frac{1}{4}(F_{\mu\nu})^2 + |D_\mu\phi|^2 - V(|\phi|), \quad (1)$$

where  $F_{\mu\nu} = \partial_\mu A_\nu - \partial_\nu A_\mu$  and  $D_\mu = \partial_\mu + igA_\mu$  are the electromagnetic field strength tensor and the gauge covariant derivative, respectively. In classically conformal models the scalar potential at classical level is quartic,  $V(|\phi|) = \lambda|\phi|^4/4$ , however, a non-trivial minimum is revealed when the radiative corrections are taken into account [103]. Finite temperature effects induce a potential energy barrier between the symmetric and the symmetry-breaking minima. The one-loop effective potential of classically conformal scalar electrodynamics is

$$V(|\phi|) = \frac{g^2}{2}T^2|\phi|^2 + \frac{3g^4}{4\pi^2}\phi^4 \left[ \ln \frac{|\phi|^2}{v^2} - \frac{1}{2} \right], \quad (2)$$

where  $T$  denotes temperature of the plasma and  $v$  the vacuum expectation value of  $|\phi|$  at  $T = 0$ .

The symmetric and broken vacua are degenerate at a temperature  $T = T_c$ . The bubble nucleation temperature  $T_n < T_c$  is defined as the temperature at which the probability of nucleating at least one bubble in a horizon volume in a Hubble time approaches unity,  $\Gamma(T_n) = H(T_n)^4$ .

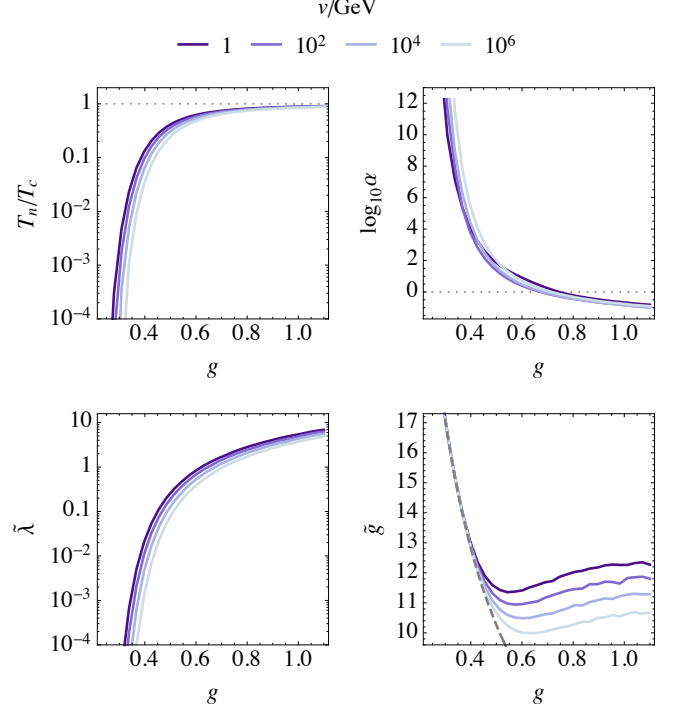


FIG. 1. The bubble nucleation temperature  $T_n$ , the strength of the transition  $\alpha$ , and the dimensionless parameters  $\tilde{\lambda}$  and  $\tilde{g}$  (see Eq. (12)) as a function of the gauge coupling  $g$ . Different curves correspond to different values of the vacuum expectation value of  $|\phi|$  as indicated at the top. The gray dashed curve in the lower right panel shows a simple approximation  $\tilde{g} = 5.13/g$  which works well in severely supercooled scenarios.

The bubble nucleation rate  $\Gamma(T)$  is given by<sup>1</sup>

$$\Gamma(T) = T^4 \left( \frac{S_3}{2\pi T} \right)^{3/2} e^{-S_3/T}, \quad (3)$$

where  $S_3$  is the action for a classical O(3) symmetric bubble configuration,

$$S_3 = 4\pi \int dr r^2 \left[ \frac{1}{2} \left( \frac{d|\phi|}{dr} \right)^2 + V(|\phi|) \right]. \quad (4)$$

In the upper panels of Fig. 1 we show the ratio  $T_n/T_c$  and the parameter  $\alpha$ , defined as

$$\alpha = \frac{\Delta V(T=0)}{\rho_{\text{rad}}(T)}, \quad (5)$$

as a function of the gauge coupling  $g$  for different values of the vacuum expectation value of  $|\phi|$ . The parameter  $\alpha$  characterizes the strength of the transition and if  $\alpha > 1$  the transition finishes only after a vacuum energy

<sup>1</sup> We have checked that indeed in this model the O(3) symmetric nucleation dominates over the O(4) symmetric one.

dominated period. We assume that only vacuum and radiation energies contribute to the expansion rate,

$$\Delta V(T=0) = \frac{3g^4 v^4}{8\pi^2}, \quad \rho_{\text{rad}}(T) = \frac{\pi^2}{90} g_*(T) T^4, \quad (6)$$

and use the Standard Model prediction for the effective number of relativistic degrees of freedom,  $g_*(T)$  [104].

### III. BUBBLE COLLISIONS

The bubble nucleation breaks the  $U(1)$  symmetry inside the bubble, as the complex phase of the scalar field, which we denote by  $\varphi$  (i.e.  $\phi = |\phi|e^{i\varphi}$ ), takes a value in the range  $0 \leq \varphi < 2\pi$ . Different bubbles in general nucleate with different complex phases such that  $\varphi$  follows a uniform probability distribution. Eventually, as the bubbles expand, they will collide with bubbles containing different complex phases. In the following we extend the work presented in [77] by assuming that the  $U(1)$  symmetry is gauged and considering the effects of the gauge field  $A_\mu$  on the evolution of the stress-energy tensor that sources GWs. The evolution is governed by the equations of motion, given in the Lorentz gauge ( $\partial_\mu A^\mu = 0$ ) by

$$\begin{aligned} \square A_\mu &= ig(\phi^* \partial_\mu \phi - \phi \partial_\mu \phi^*) - 2g^2 A_\mu |\phi|^2, \\ \square \phi + \frac{dV}{d\phi^*} &= -i2gA_\mu \partial^\mu \phi + g^2 A^2 \phi, \\ \square \phi^* + \frac{dV}{d\phi} &= i2gA_\mu \partial^\mu \phi^* + g^2 A^2 \phi^*, \end{aligned} \quad (7)$$

which we next solve on a lattice for two-bubble collisions.

As shown in Ref. [75], for the late evolution of the bubbles, and in particular for the evolution after bubble collisions, it does not matter whether the initial bubbles are  $O(3)$  or  $O(4)$  symmetric. Although in the scenario described above the bubbles nucleate with only  $O(3)$  symmetry, in the following we simulate two-bubble collisions starting from  $O(4)$  symmetric initial bubbles, as the system in this case has one degree of freedom less and the simulations are therefore significantly faster.

The radial profile of an  $O(4)$  symmetric initial configuration is obtained as the solution of

$$\partial_r^2 |\phi| + \frac{3}{r} \partial_r |\phi| = \frac{dV}{d|\phi|} \quad (8)$$

with boundary conditions  $\partial_r |\phi| = 0$  at  $r = 0$  and  $|\phi| \rightarrow 0$  at  $r \rightarrow \infty$ . We start from a configuration where  $A_\mu = 0$ <sup>2</sup> and two  $O(4)$  symmetric scalar field bubbles have nucleated simultaneously at  $(x, y, z) = (0, 0, \pm d/2)$ , where  $d$  denotes their mutual distance. This system is conveniently described in coordinates  $(s, z, \psi, \theta)$  defined via  $\tan \theta = x/y$ ,  $t = s \cosh \psi$  and  $r = s \sinh \psi$  where  $r^2 = x^2 + y^2$ .<sup>3</sup> The d'Alembertian in these coordinates reads

$$\square X = \partial_s^2 X + \frac{2}{s} \partial_s X - \partial_z^2 X. \quad (9)$$

and, in dimensionless variables,  $\phi' = \phi/v$ ,  $A' = A/v$ ,  $x'^\mu = \sqrt{\Delta V} x^\mu/v$ , the equations of motion (7) take the form

$$\begin{aligned} \square' A'_{s,z} &= \tilde{g}(\phi'_I \partial'_{s,z} \phi'_R - \phi'_R \partial'_{s,z} \phi'_I) - \tilde{g}^2 A'_{s,z} (\phi'_R^2 + \phi'_I^2), \\ \square' \phi'_R + \frac{dV'}{d\phi'_R} &= 2\tilde{g}(A'_s \partial'_s \phi'_I - A'_z \partial'_z \phi'_I) + \tilde{g}^2 (A'_s^2 - A'_z^2) \phi'_R, \\ \square' \phi'_I + \frac{dV'}{d\phi'_I} &= -2\tilde{g}(A'_s \partial'_s \phi'_R - A'_z \partial'_z \phi'_R) + \tilde{g}^2 (A'_s^2 - A'_z^2) \phi'_I, \end{aligned} \quad (10)$$

where  $\phi_R$  and  $\phi_I$  are the real and imaginary parts of  $\phi$ , defined such that  $\phi = (\phi_R + i\phi_I)/\sqrt{2}$ .

The dimensionless scalar potential  $V' = V/\Delta V$ , where  $\Delta V$  denotes the vacuum energy difference between the

symmetric and broken vacua at temperature  $T$ , can be written as

$$V'(\phi') = \tilde{\lambda} |\phi'|^2 + |\phi'|^4 \left[ (\tilde{\lambda} + 2) \ln |\phi'|^2 - (\tilde{\lambda} + 1) \right]. \quad (11)$$

We have defined dimensionless parameters  $\tilde{g}$  and  $\tilde{\lambda}$  as

$$\tilde{g} = \frac{gv^2}{\sqrt{\Delta V}}, \quad \tilde{\lambda} = \frac{g^2 v^2 T^2}{2\Delta V}, \quad (12)$$

such that  $\tilde{\lambda}$  determines the shape of the scalar potential and  $\tilde{g}$  the strength of the coupling between the gauge field and the scalar field.

In the lower panels of Fig. 1 we show the parameters  $\tilde{\lambda}$  and  $\tilde{g}$  at  $T = T_n$  as a function of  $g$  for different values of

<sup>2</sup> The gauge field acquires a mass term  $\propto g^2 T^2 A^2$  through thermal corrections, and therefore  $A_\mu = 0$  is the vacuum configuration. We have checked that the thermal mass of  $A_\mu$  does not affect the dynamics of the system in the parameter range of interest, and therefore we don't write it explicitly into the equations of motion.

<sup>3</sup> We consider the region  $t > r$  as this is where the bubbles collide (see Ref. [75] for details).

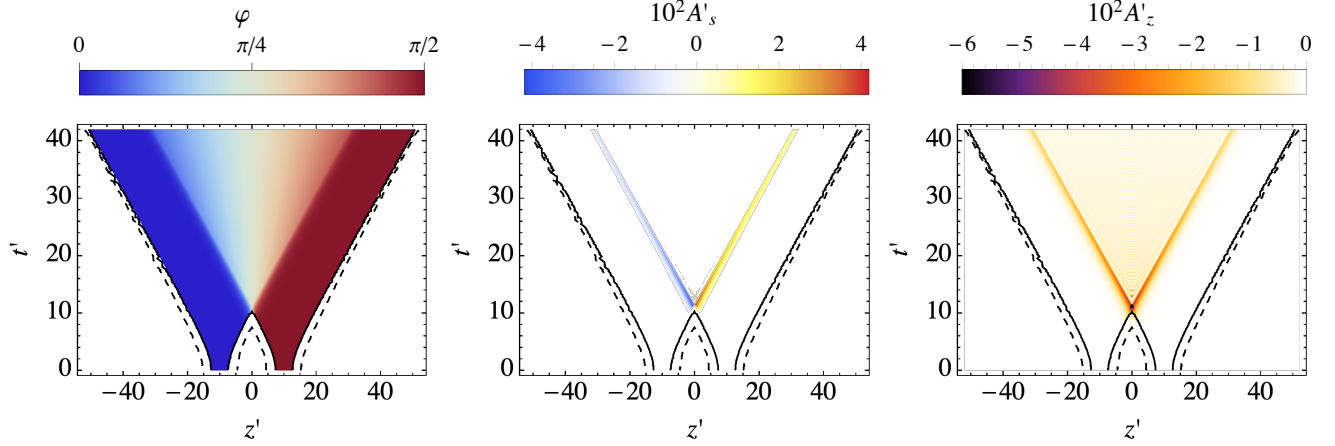


FIG. 2. Collision of two bubbles with initial complex phase difference  $\Delta\varphi = \pi/2$ . The solid and dashed curves correspond to  $|\phi'| = 0.1$  and  $|\phi'| = 0.01$ , respectively. The color coding indicates in the left panel the complex phase of the scalar field, in the middle panel the  $s$  component of the gauge field and in the right panel the  $z$  component of the gauge field.

v. If the bubble nucleation happens at  $T_n \ll T_c$  (i.e. if the transition is strongly supercooled), then  $\tilde{g} \approx 5.13/g$  as shown by the dashed gray curve in the lower right panel. This approximation is obtained by taking  $\Delta V = \Delta V(T = 0)$  in the definition of  $\tilde{g}$ . Moreover, in this limit  $\tilde{\lambda}^2 = 60/(g_*(T_n)\alpha)$ , and therefore it is clear that  $\tilde{\lambda} \ll 1$  if  $\alpha \gg 1$ .

We solve the equations of motion (10) numerically on a diamond-shaped  $sz$  lattice as in Ref. [105]. In Fig. 2 we show the result from a simulation with  $\tilde{\lambda} = 0.04$ ,  $\tilde{g} = 10$ , initial bubble separation  $d' = 20$  (in the dimensionless units) and initial complex phase difference  $\Delta\varphi = \pi/2$ . The left panel shows the evolution of the complex phase of the scalar field. As can be seen from the equations of motion (10), gradients in  $\varphi$  source the gauge field. Therefore, it is expected that the gauge field deviates from zero where the gradients in  $\varphi$  are large. We see this in the middle and right panels of Fig. 2, which show the gauge field components  $A_s$  and  $A_z$ : A sharp feature in the gauge field propagates roughly at the speed of light after collision.

#### IV. GRAVITATIONAL WAVE SOURCE

Next we will study how the GW source scales in bubble collisions. The total energy spectrum in a direction  $\hat{k}$  at an angular frequency  $\omega = |\vec{k}|$  of the GWs emitted in the phase transition is given by [106]

$$\frac{dE}{d\Omega_k d\omega} = 2G\omega^2 \Lambda_{ij,lm}(\hat{k}) T_{ij}^*(\vec{k}) T_{lm}(\vec{k}), \quad (13)$$

where  $\Lambda_{ij,lm}$  is the transverse-traceless projection tensor. As  $\Lambda_{ij,lm} \delta_{ij} = 0$ , the part of the stress energy tensor that is proportional to the metric tensor  $g_{\mu\nu}$  does not contribute to formation of GWs. We therefore define

$T_{\mu\nu}$  as

$$T_{\mu\nu} \equiv \left( \frac{\partial \mathcal{L}}{\partial(\partial^\mu \phi)} \partial_\nu \phi + \text{c.c.} \right) + \frac{\partial \mathcal{L}}{\partial(\partial^\mu A_\alpha)} \partial_\nu A_\alpha. \quad (14)$$

Continuing the study of two-bubble collisions, we now calculate  $T_{\mu\nu}$  in the simulations discussed in the previous section. Along the collision axis  $T_{zz}$  is the only non-zero component of  $T_{ij}$ . In the dimensionless variables it is given by

$$T'_{zz} = (\partial'_z \phi'_R)^2 + (\partial'_z \phi'_I)^2 - \partial'_z A'_s (\partial'_z A'_s - \partial'_s A'_z) + \tilde{g} A'_z (\phi'_I \partial'_z \phi'_R - \phi'_R \partial'_z \phi'_I). \quad (15)$$

In Fig. 3 we show the  $T'_{zz}$  by the color coding for three different two-bubble collisions. In the left panel  $\tilde{g} = 0$  and in the right panel  $\Delta\varphi = 0$ . In these cases only the scalar field gradients contribute to  $T'_{zz}$ , and the result agrees with the ones shown in Ref. [77]: If there is a complex phase difference between the colliding bubbles, the scalar field gradients propagate much longer after the collision than in the case where the complex phases are equal. The middle panel of Fig. 3 shows the case where the complex phases are different and  $\tilde{g} > 0$ . We see that the result in that case roughly matches with the  $\Delta\varphi = 0$  case. This can be understood as decay of the gradients in the complex phase of the scalar field to gauge fields.

In Fig. 4 we show by the solid curves the scaling of the maximal  $T'_{zz}$  as a function of time, averaged over simulations of different initial complex phase differences,  $\Delta\varphi$ . Two important remarks are in order: First, we see that the steep drop after the collision becomes shorter as  $\tilde{\lambda}$  decreases. This can be traced to false vacuum trapping, i.e. field bouncing back to the false vacuum in the collision region, which becomes increasingly likely for larger values of  $\tilde{\lambda}$ .<sup>4</sup> Second, the larger  $\tilde{g}$  is, the closer the be-

<sup>4</sup> We note that in Ref. [77] we studied rather large values of  $\tilde{\lambda}$  and

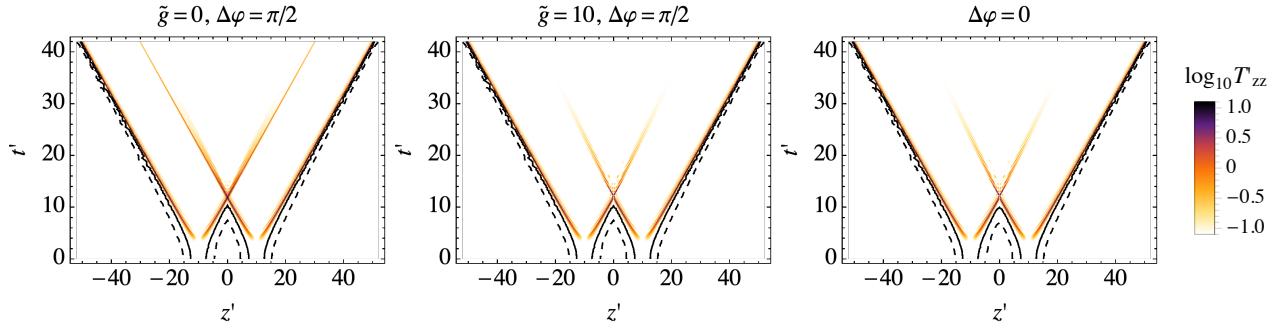


FIG. 3. Collision of two bubbles with values of  $\Delta\varphi$  and  $\tilde{g}$  indicated above the plots, and  $\tilde{\lambda} = 0.04$ . For the  $\Delta\varphi = 0$  case the value of  $\tilde{g}$  is irrelevant. The solid and dashed curves correspond to  $|\phi'| = 0.1$  and  $|\phi'| = 0.01$ , respectively, and the color coding indicates the value of the  $zz$  component of the stress energy tensor.

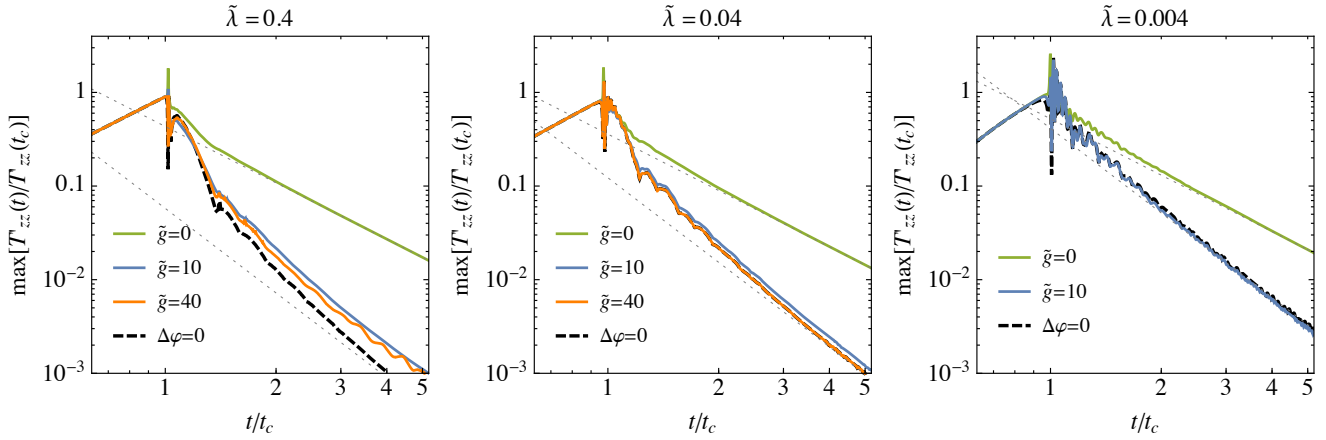


FIG. 4. Evolution of the GW source in collision of two bubbles averaged over simulations with different initial complex phase differences (with initial distance  $d = 40$ ). Different solid curves correspond to different values of  $\tilde{g}$ , and different panels correspond to different values of  $\tilde{\lambda}$ . The black dashed curve corresponds to  $\Delta\varphi = 0$ , and the dotted lines show  $\propto t^{-2}$  and  $\propto t^{-3}$  power-laws.

haviour of the GW source is to the case  $\Delta\varphi = 0$ , which for  $t \gg t_c$  scales as  $\propto t^{-3}$ . Moreover, the smaller  $\tilde{\lambda}$  is, the faster the scaling reaches the  $\Delta\varphi = 0$  case as a function of  $\tilde{g}$ . From Fig. 1 we see that  $\tilde{\lambda}$  is very small,  $\tilde{\lambda} \ll 1$ , and  $\tilde{g}$  is large,  $\tilde{g} > 10$ , in the region where supercooling is strong and the bubble collision signal we discuss can be the dominant contribution. Therefore, in the following we simply use  $\propto t^{-3}$  scaling for the GW source after the collision. We will also study  $\propto t^{-2}$  scaling which can be realized e.g. in models with a global U(1) symmetry.

## V. GRAVITATIONAL WAVE SPECTRUM

Knowing the scaling of the GW source in two-bubble collisions, we are ready to calculate the GW spectrum from a phase transition.<sup>5</sup> We consider the exponential bubble nucleation rate per unit volume,  $\Gamma \propto e^{\beta t}$ . Similarly as in Ref. [77], we write the abundance of GWs produced in bubble collisions in a logarithmic frequency interval as

$$\Omega_{\text{GW}}(\omega) \equiv \frac{1}{E_{\text{tot}}} \frac{dE}{d\ln\omega} = \left(\frac{H}{\beta}\right)^2 \left(\frac{\alpha}{1+\alpha}\right)^2 S(\omega), \quad (16)$$

where

$$S(\omega) = \left(\frac{\omega}{\beta}\right)^3 \frac{3\beta^5}{8\pi V_s} \int d\Omega_k [|C_+(\omega)|^2 + |C_\times(\omega)|^2] \quad (17)$$

therefore saw similar drop as in the left panel of Fig. 4. Thus, the results of [77] hold only for  $\sqrt{\tilde{\lambda}} = \kappa = \mathcal{O}(0.1)$  while here we will extend them to  $\tilde{\lambda} \ll 1$  which is more relevant for supercooled collisions where the bubble collision GW signal can be strong.

<sup>5</sup> We have also checked that subsequent collisions of the collided parts do not change the scaling.

gives the spectral shape of the GW background. The volume over which  $\Omega_{\text{GW}}$  is averaged is denoted by  $V_s$ . The functions  $C_{+,\times}$  are for  $\hat{k} = (0, 0, 1)$ , in the thin wall limit, given by (see Appendix A)

$$C_{+,\times}(\omega) \approx \frac{1}{6\pi} \sum_n \int_{t_n} dt d\Omega_x \sin^2 \theta_x g_{+,\times}(\phi_x) \times R_n^3 f(R_n) e^{i\omega(t-z_n-R_n \cos \theta_x)}, \quad (18)$$

where  $t_n$  denotes the nucleation time of the bubble  $n$ ,  $z_n$  the  $z$  coordinate of the bubble nucleation center,  $R_n = t - t_n$  the bubble radius at time  $t > t_n$ , and the functions  $g_{+,\times}$  are defined as  $g_+(\phi_x) = \cos(2\phi_x)$  and  $g_\times(\phi_x) = \sin(2\phi_x)$ . The function  $f(R_n)$  accounts for the scaling of the GW source and depends on the time when the bubble wall element collided with another bubble. The function  $f(R_n)$  is (see Appendix A)

$$f(R_n) = \begin{cases} 1, & R \leq R_{n,c}, \\ (R_{n,c}/R_n)^{\xi+1}, & R > R_{n,c}, \end{cases} \quad (19)$$

where  $R_{n,c}$  denotes the bubble radius at the time of the collision and we model the scaling of the GW source after the collision with a power-law,

$$\frac{\max[T_{zz}(R_n)]}{\max[T_{zz}(R_{n,c})]} \approx \left( \frac{R_{n,c}}{R_n} \right)^\xi. \quad (20)$$

As discussed in the previous section,  $\xi = 3$  in the case of breaking of a gauge U(1) symmetry. The envelope approximation [72] corresponds to  $f(R_n > R_{n,c}) = 0$ , which is obtained in the limit  $\xi \rightarrow \infty$ .

We calculate the GW spectrum  $S$  in the same way as in Ref. [77]: We nucleate bubbles in a box of volume  $V_s$  according to the rate  $\Gamma \propto e^{\beta t}$ , discretise the bubble surfaces, find when each of the bubble surface elements collides with another bubble wall, and integrate over the bubble surfaces and sum over all bubbles as in Eq. (18). We perform the time integral analytically, as  $f$  is in our approximation simply a piecewise power-law. Since our simulation volume is a cubic box, we can perform the integral in Eq. (17) over six  $\hat{k}$  directions by performing rotations of the simulation box. Finally, we perform many of these simulations with different random realizations of the bubble nucleation history. Our results are calculated from 40 simulations of cubic box size  $12\beta$ .

We parametrize our results as a broken power-law fit for the spectrum is given by

$$S_{\text{fit}}(\omega) = \frac{\bar{S} (a+b)^c}{\left[ b \left( \frac{\omega}{\bar{\omega}} \right)^{-a/c} + a \left( \frac{\omega}{\bar{\omega}} \right)^{b/c} \right]^c}, \quad (21)$$

where  $\bar{S}$  and  $\bar{\omega}$  are the peak amplitude and angular frequency of the spectrum,  $a, b > 0$  are the low- and high-frequency slopes of the spectrum respectively, and  $c$  determines the width of the peak. We show the parameter values and their errors resulting from fits to our simulation results in Table I for  $\xi = 2$ ,  $\xi = 3$  and  $\xi = 4$  as well

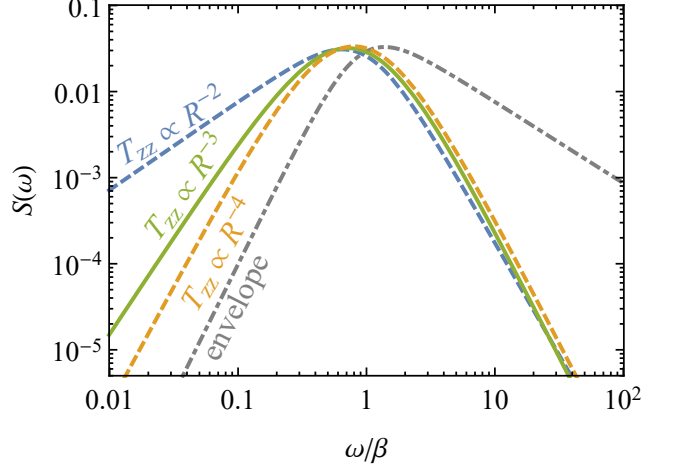


FIG. 5. The spectral shape of GWs from bubble collisions (see Eq. (16) for definition of  $S(\omega)$ ). The curves show broken power-law fits to the simulation results for different decay-laws of the GW source after collisions ( $T_{zz} \propto R^{-\xi}$ ) and in envelope approximation. The solid curve with  $T_{zz} \propto R^{-3}$  is realised in most of the relevant parameter space. The corresponding parameters of the fit, and their errors, are given in Table I.

	$100\bar{S}$	$\bar{\omega}/\beta$	$a$	$b$	$c$
$\xi = 2$	$3.1 \pm 0.1$	$0.64 \pm 0.01$	$1.00 \pm 0.01$	$2.61 \pm 0.06$	$1.5 \pm 0.1$
$\xi = 3$	$3.2 \pm 0.1$	$0.71 \pm 0.01$	$2.25 \pm 0.02$	$2.94 \pm 0.02$	$3.5 \pm 0.1$
$\xi = 4$	$3.3 \pm 0.1$	$0.80 \pm 0.01$	$2.78 \pm 0.02$	$2.91 \pm 0.02$	$3.9 \pm 0.1$
env.	$3.3 \pm 0.1$	$1.38 \pm 0.03$	$3.01 \pm 0.01$	$0.94 \pm 0.03$	$1.5 \pm 0.1$

TABLE I. Fitted values of the parametrization (21) for  $\xi = 2$ ,  $\xi = 3$  and  $\xi = 4$  (see Eq. (19)) as well as in the envelope approximation.

as for the envelope approximation, and illustrate these fits in Fig. 5.

As discussed in the previous section,  $\xi = 2$  correspond to  $\tilde{g} \ll 1$ , and  $\xi = 3$  to  $\tilde{g} \gg 1$ . In these cases we find, respectively,  $\propto \omega^{1.0}$  and  $\propto \omega^{2.3}$  low- and  $\propto \omega^{-2.6}$  and  $\propto \omega^{-2.9}$  high-frequency behaviours. The spectrum in both cases peaks slightly below  $\omega = \beta$  with an amplitude  $S \approx 0.03$ . We show for comparison also the case where  $\xi = 4$ . We find that increasing  $\xi$  brings the low-frequency power-law quickly closer to envelope result,  $a = 3.0$ . The high-frequency tail instead seems to decrease very slowly for  $\xi > 3$ .<sup>6</sup> Getting a high-frequency tail that agrees with the envelope approximation, which corresponds to the limit  $\xi \rightarrow \infty$  and gives  $b = 0.9$ , therefore seems to require very rapid decay of the GW source after the bubble collisions,  $\xi \gg 1$ .

<sup>6</sup> We have also calculated the spectrum for  $\xi = 5$  in which case  $a = 2.96$  and  $b = 2.85$ .

## VI. CONCLUSIONS

Gravitational waves (GWs) from a cosmological first-order phase transition are dominantly sourced by bubble collisions if the phase transition is sufficiently strongly supercooled. This can be realized in models featuring scale invariance at classical level. The simplest realistic examples of such involve breaking of a U(1) gauge symmetry. Motivated by these observations, we have studied the formation of GWs in a first-order phase transition in classically conformal scalar electrodynamics.

We have estimated the GW spectrum by first studying the scaling of the GW source in lattice simulations of two-bubble collisions, and then using that scaling in many-bubble simulations in the thin-wall limit. We have found that the presence of the gauge field brings the results close to the simple real scalar case with the field gradients sourcing GWs decaying with the bubble size as  $T_{zz} \propto R^{-3}$ . The resulting spectrum follows  $\Omega_{\text{GW}} \propto \omega^{2.3}$  at low frequencies and  $\Omega_{\text{GW}} \propto \omega^{-2.9}$  at high frequencies. The spectrum in this case is shown by the green solid curve in Fig. 5. By calculating the transition temperature in our classically conformal scalar electrodynamics potential we have shown that this limit with  $\tilde{\lambda} \ll 1$  and  $\tilde{g} \gg 1$  is realised in most of the parameter space of interest where the transition is very strong and the bubble collision signal that we discussed can give the dominant contribution to the GW spectrum.

While our result should describe both real and gauged scalar field transitions we have nevertheless explored also different energy decay laws which could be realised in other models. Most notably,  $T_{zz} \propto R^{-2}$  can be possibly realised in models where the U(1) symmetry is global (i.e.  $\tilde{g} = 0$ ) or modified transition dynamics allow  $\tilde{g} \ll 1$ . In this case the resulting spectrum would follow  $\Omega_{\text{GW}} \propto \omega$  at low frequencies and  $\Omega_{\text{GW}} \propto \omega^{2.6}$  at high frequencies. Exploring the other possibilities we also have shown that the envelope result is unlikely to be able to describe realistic spectra especially at high frequencies.

## ACKNOWLEDGMENTS

ML was supported by the Polish National Science Center grant 2018/31/D/ST2/02048 and VV by Juan de la Cierva fellowship from Spanish State Research Agency. The project is co-financed by the Polish National Agency for Academic Exchange within Polish Returns Programme under agreement PPN/PPO/2020/1/00013/U/00001. This work was also supported by the grants FPA2017-88915-P and SEV-2016-0588. IFAE is partially funded by the CERCA program of the Generalitat de Catalunya.

## Appendix A: Thin-wall approximation

In this appendix we generalize the treatment of Ref. [77] to the case where the stress-energy tensor is not given solely by the scalar field gradients after the bubble collisions. The Fourier transform of the stress-energy tensor is given by

$$T_{ij}(\vec{k}) = \frac{1}{2\pi} \int dt d^3x e^{i\omega t - i\vec{k} \cdot \vec{x}} T_{ij}(x). \quad (\text{A1})$$

By breaking the spatial integral into regions around each bubble nucleation center and taking  $\vec{k} = (0, 0, \omega)$ , we get

$$T_{ij}(\vec{k}) = \frac{1}{2\pi} \sum_n \int_{t_n} dt d\Omega_x e^{i\omega(t - z_n - R_n \cos \theta_x)} \int dr r^2 T_{ij}(r), \quad (\text{A2})$$

where  $t_n$  denotes the nucleation time of the bubble  $n$ ,  $z_n$  the  $z$  coordinate of the bubble nucleation center, and  $R_n = t - t_n$  the bubble radius at time  $t > t_n$ . It is convenient to write  $T_{ij}(r)$  in a coordinate system where the  $z$  axis points to the radial direction,  $\hat{z} = \hat{r}$ . The coordinate transformation of  $T_{ij}(r)$  is

$$T_{ij}(r) = T_{i'j'}(r) \frac{\partial x_{i'}}{\partial x_i} \frac{\partial x_{j'}}{\partial x_j}. \quad (\text{A3})$$

If only  $zz$  component of is non zero, we get

$$\int dr r^2 T_{ij}(r) = \hat{x}_i \hat{x}_j \int dr r^2 T_{zz}(r). \quad (\text{A4})$$

In the thin-wall limit we approximate

$$\begin{aligned} \int dr r^2 T_{zz}(r) &\approx LR_n^2 \max[T_{zz}(R_n)] \\ &\equiv \frac{\Delta V}{3} R_n^3 f(R_n), \end{aligned} \quad (\text{A5})$$

where  $L$  denotes the bubble wall width.

Before the wall element in the solid angle  $d\Omega$  collides with another bubble  $T_{zz}$  is given solely by the scalar field gradients,  $T_{zz} = |\partial_z \phi|^2$ . By energy conservation

$$\int dr r^2 |\partial_z \phi|^2 = \frac{\Delta V}{3} R_n^3, \quad (\text{A6})$$

where  $R_{n,c}$  denotes the bubble radius at the time of the collision. Therefore, before the collision

$$f(R_n \leq R_{n,c}) = 1. \quad (\text{A7})$$

From the definition of  $f$  and using  $f(R_n = R_{n,c}) = 1$  we get that the wall width at the collision moment is

$$L_c = \frac{\Delta V}{3 \max[T_{zz}(R_{n,c})]} R_{n,c}. \quad (\text{A8})$$

Before the collision the bubble wall gets thinner as the Lorentz factor of the bubble wall increases, but after the collision the wall element moves roughly at a constant

velocity as no more energy is injected into it. Therefore we assume that after the collision the wall thickness  $L$  remains constant,  $L = L_c$ . We can then write the  $f(R_n)$  function after the collision as

$$\begin{aligned} f(R_n > R_{n,c}) &= \frac{3L_c \max[T_{zz}(R_n)]}{R_n \Delta V} \\ &= \frac{R_{n,c}}{R_n} \frac{\max[T_{zz}(R_n)]}{\max[T_{zz}(R_{n,c})]}. \end{aligned} \quad (\text{A9})$$

Finally, since  $T_{ij}(\vec{k})$  is symmetric, we can write the transverse-traceless projection for  $\hat{k} = (0, 0, 1)$  as

$$2\Lambda_{ij,lm}T_{ij}^*(\vec{k})T_{lm}(\vec{k}) = \Delta V^2 (|C_+(\omega)|^2 + |C_\times(\omega)|^2). \quad (\text{A10})$$

The functions  $C_+ \equiv T_{11} - T_{22}$  and  $C_\times \equiv 2T_{12}$  are given by

$$\begin{aligned} C_{+,\times}(\omega) &\approx \frac{1}{6\pi} \sum_n \int_{t_n} dt d\Omega_x \sin^2 \theta_x g_{+,\times}(\phi_x) \\ &\quad \times R_n^3 f(R_n) e^{i\omega(t-z_n - R_n \cos \theta_x)}, \end{aligned} \quad (\text{A11})$$

where  $g_+(\phi_x) = \cos(2\phi_x)$  and  $g_\times(\phi_x) = \sin(2\phi_x)$ .

## REFERENCES

- [1] B. Abbott *et al.* (LIGO Scientific, Virgo), Phys. Rev. Lett. **119**, 161101 (2017), arXiv:1710.05832 [gr-qc].
- [2] R. Abbott *et al.* (LIGO Scientific, Virgo), (2020), arXiv:2010.14527 [gr-qc].
- [3] M. Punturo *et al.*, Class. Quant. Grav. **27**, 194002 (2010).
- [4] S. Hild *et al.*, Class. Quant. Grav. **28**, 094013 (2011), arXiv:1012.0908 [gr-qc].
- [5] G. Janssen *et al.*, PoS **AASKA14**, 037 (2015), arXiv:1501.00127 [astro-ph.IM].
- [6] P. W. Graham, J. M. Hogan, M. A. Kasevich, and S. Rajendran, Phys. Rev. **D94**, 104022 (2016), arXiv:1606.01860 [physics.atom-ph].
- [7] H. Audley *et al.* (LISA), (2017), arXiv:1702.00786 [astro-ph.IM].
- [8] P. W. Graham, J. M. Hogan, M. A. Kasevich, S. Rajendran, and R. W. Romani (MAGIS), (2017), arXiv:1711.02225 [astro-ph.IM].
- [9] L. Badurina *et al.*, JCAP **05**, 011 (2020), arXiv:1911.11755 [astro-ph.CO].
- [10] Y. A. El-Neaj *et al.* (AEDGE), EPJ Quant. Technol. **7**, 6 (2020), arXiv:1908.00802 [gr-qc].
- [11] Z. Arzoumanian *et al.* (NANOGrav), (2020), arXiv:2009.04496 [astro-ph.HE].
- [12] J. Ellis and M. Lewicki, (2020), arXiv:2009.06555 [astro-ph.CO].
- [13] S. Blasi, V. Brdar, and K. Schmitz, (2020), arXiv:2009.06607 [astro-ph.CO].
- [14] V. Vaskonen and H. Veermäe, (2020), arXiv:2009.07832 [astro-ph.CO].
- [15] V. De Luca, G. Franciolini, and A. Riotto, (2020), arXiv:2009.08268 [astro-ph.CO].
- [16] Y. Nakai, M. Suzuki, F. Takahashi, and M. Yamada, (2020), arXiv:2009.09754 [astro-ph.CO].
- [17] W. Ratzinger and P. Schwaller, (2020), arXiv:2009.11875 [astro-ph.CO].
- [18] K. Kohri and T. Terada, (2020), arXiv:2009.11853 [astro-ph.CO].
- [19] S. Vagnozzi, (2020), arXiv:2009.13432 [astro-ph.CO].
- [20] A. Neronov, A. Roper Pol, C. Caprini, and D. Semikoz, (2020), arXiv:2009.14174 [astro-ph.CO].
- [21] H. Middleton, A. Sesana, S. Chen, A. Vecchio, W. Del Pozzo, and P. Rosado, (2020), arXiv:2011.01246 [astro-ph.HE].
- [22] E. Witten, Phys. Rev. **D30**, 272 (1984).
- [23] C. Grojean and G. Servant, Phys. Rev. **D75**, 043507 (2007), arXiv:hep-ph/0607107 [hep-ph].
- [24] J. Espinosa, T. Konstandin, J. No, and M. Quiros, Phys. Rev. D **78**, 123528 (2008), arXiv:0809.3215 [hep-ph].
- [25] G. C. Dorsch, S. J. Huber, and J. M. No, Phys. Rev. Lett. **113**, 121801 (2014), arXiv:1403.5583 [hep-ph].
- [26] J. Jaeckel, V. V. Khoze, and M. Spannowsky, Phys. Rev. **D94**, 103519 (2016), arXiv:1602.03901 [hep-ph].
- [27] R. Jinno and M. Takimoto, Phys. Rev. D **95**, 015020 (2017), arXiv:1604.05035 [hep-ph].
- [28] M. Chala, G. Nardini, and I. Sobolev, Phys. Rev. **D94**, 055006 (2016), arXiv:1605.08663 [hep-ph].
- [29] M. Chala, M. Ramos, and M. Spannowsky, Eur. Phys. J. **C79**, 156 (2019), arXiv:1812.01901 [hep-ph].
- [30] M. Artymowski, M. Lewicki, and J. D. Wells, JHEP **03**, 066 (2017), arXiv:1609.07143 [hep-ph].
- [31] K. Hashino, M. Kakizaki, S. Kanemura, P. Ko, and T. Matsui, Phys. Lett. **B766**, 49 (2017), arXiv:1609.00297 [hep-ph].
- [32] V. Vaskonen, Phys. Rev. D **95**, 123515 (2017), arXiv:1611.02073 [hep-ph].
- [33] G. Dorsch, S. Huber, T. Konstandin, and J. No, JCAP **05**, 052 (2017), arXiv:1611.05874 [hep-ph].
- [34] A. Beniwal, M. Lewicki, J. D. Wells, M. White, and A. G. Williams, JHEP **08**, 108 (2017), arXiv:1702.06124 [hep-ph].
- [35] I. Baldes, JCAP **05**, 028 (2017), arXiv:1702.02117 [hep-ph].
- [36] L. Marzola, A. Racioppi, and V. Vaskonen, Eur. Phys. J. **C77**, 484 (2017), arXiv:1704.01034 [hep-ph].
- [37] Z. Kang, P. Ko, and T. Matsui, JHEP **02**, 115 (2018), arXiv:1706.09721 [hep-ph].
- [38] S. Iso, P. D. Serpico, and K. Shimada, Phys. Rev. Lett. **119**, 141301 (2017), arXiv:1704.04955 [hep-ph].
- [39] M. Chala, C. Krause, and G. Nardini, JHEP **07**, 062 (2018), arXiv:1802.02168 [hep-ph].
- [40] S. Bruggisser, B. Von Harling, O. Matsedonskyi, and G. Servant, JHEP **12**, 099 (2018), arXiv:1804.07314 [hep-ph].
- [41] E. Megias, G. Nardini, and M. Quiros, JHEP **09**, 095 (2018), arXiv:1806.04877 [hep-ph].
- [42] D. Croon, V. Sanz, and G. White, JHEP **08**, 203 (2018), arXiv:1806.02332 [hep-ph].
- [43] A. Alves, T. Ghosh, H.-K. Guo, K. Sinha, and D. Vagie, JHEP **04**, 052 (2019), arXiv:1812.09333 [hep-ph].
- [44] P. Baratella, A. Pomarol, and F. Rompineve, JHEP **03**, 100 (2019), arXiv:1812.06996 [hep-ph].
- [45] A. Angelescu and P. Huang, Phys. Rev. **D99**, 055023 (2019), arXiv:1812.08293 [hep-ph].
- [46] D. Croon, T. E. Gonzalo, and G. White, JHEP **02**, 083 (2019), arXiv:1812.02747 [hep-ph].
- [47] V. Brdar, A. J. Helmboldt, and J. Kubo, JCAP **1902**,

- 021 (2019), arXiv:1810.12306 [hep-ph].
- [48] A. Beniwal, M. Lewicki, M. White, and A. G. Williams, JHEP **02**, 183 (2019), arXiv:1810.02380 [hep-ph].
- [49] M. Breitbach, J. Kopp, E. Madge, T. Opferkuch, and P. Schwaller, JCAP **07**, 007 (2019), arXiv:1811.11175 [hep-ph].
- [50] C. Marzo, L. Marzola, and V. Vaskonen, Eur. Phys. J. **C79**, 601 (2019), arXiv:1811.11169 [hep-ph].
- [51] I. Baldes and C. Garcia-Cely, JHEP **05**, 190 (2019), arXiv:1809.01198 [hep-ph].
- [52] T. Prokopec, J. Rezacek, and B. Swiezewska, JCAP **1902**, 009 (2019), arXiv:1809.11129 [hep-ph].
- [53] M. Fairbairn, E. Hardy, and A. Wickens, JHEP **07**, 044 (2019), arXiv:1901.11038 [hep-ph].
- [54] A. J. Helmboldt, J. Kubo, and S. van der Woude, Phys. Rev. **D100**, 055025 (2019), arXiv:1904.07891 [hep-ph].
- [55] P. S. B. Dev, F. Ferrer, Y. Zhang, and Y. Zhang, JCAP **1911**, 006 (2019), arXiv:1905.00891 [hep-ph].
- [56] S. A. R. Ellis, S. Ipek, and G. White, JHEP **08**, 002 (2019), arXiv:1905.11994 [hep-ph].
- [57] R. Jinno, T. Konstandin, and M. Takimoto, JCAP **1909**, 035 (2019), arXiv:1906.02588 [hep-ph].
- [58] J. Ellis, M. Fairbairn, M. Lewicki, V. Vaskonen, and A. Wickens, JCAP **1909**, 019 (2019), arXiv:1907.04315 [astro-ph.CO].
- [59] A. Azatov, D. Barducci, and F. Sgarlata, JCAP **07**, 027 (2020), arXiv:1910.01124 [hep-ph].
- [60] B. Von Harling, A. Pomarol, O. Pujolàs, and F. Rompineve, (2019), arXiv:1912.07587 [hep-ph].
- [61] L. Delle Rose, G. Panico, M. Redi, and A. Tesi, JHEP **04**, 025 (2020), arXiv:1912.06139 [hep-ph].
- [62] M. Barroso Mancha, T. Prokopec, and B. Swiezewska, (2020), arXiv:2005.10875 [hep-th].
- [63] A. Azatov and M. Vanvlasselaer, (2020), arXiv:2010.02590 [hep-ph].
- [64] F. Giese, T. Konstandin, K. Schmitz, and J. Van De Vis, (2020), arXiv:2010.09744 [astro-ph.CO].
- [65] S. Hoeche, J. Kozaczuk, A. J. Long, J. Turner, and Y. Wang, (2020), arXiv:2007.10343 [hep-ph].
- [66] D. Croon, O. Gould, P. Schicho, T. V. Tenkanen, and G. White, (2020), arXiv:2009.10080 [hep-ph].
- [67] F. R. Ares, M. Hindmarsh, C. Hoyos, and N. Jokela, (2020), arXiv:2011.12878 [hep-th].
- [68] R.-G. Cai and S.-J. Wang, (2020), arXiv:2011.11451 [astro-ph.CO].
- [69] S. R. Coleman, Phys. Rev. **D15**, 2929 (1977), [Erratum: Phys. Rev. D16, 1248 (1977)].
- [70] C. G. Callan, Jr. and S. R. Coleman, Phys. Rev. **D16**, 1762 (1977).
- [71] A. D. Linde, Nucl. Phys. **B216**, 421 (1983), [Erratum: Nucl. Phys. B223, 544 (1983)].
- [72] A. Kosowsky and M. S. Turner, Phys. Rev. **D47**, 4372 (1993), arXiv:astro-ph/9211004 [astro-ph].
- [73] D. Cutting, M. Hindmarsh, and D. J. Weir, Phys. Rev. **D97**, 123513 (2018), arXiv:1802.05712 [astro-ph.CO].
- [74] J. Ellis, M. Lewicki, J. M. No, and V. Vaskonen, JCAP **1906**, 024 (2019), arXiv:1903.09642 [hep-ph].
- [75] M. Lewicki and V. Vaskonen, Phys. Dark Universe **30**, 100672 (2020), arXiv:1912.00997 [astro-ph.CO].
- [76] D. Cutting, E. G. Escartin, M. Hindmarsh, and D. J. Weir, (2020), arXiv:2005.13537 [astro-ph.CO].
- [77] M. Lewicki and V. Vaskonen, Eur. Phys. J. C **80**, 1003 (2020), arXiv:2007.04967 [astro-ph.CO].
- [78] M. Kamionkowski, A. Kosowsky, and M. S. Turner, Phys. Rev. D **49**, 2837 (1994), arXiv:astro-ph/9310044.
- [79] M. Hindmarsh, S. J. Huber, K. Rummukainen, and D. J. Weir, Phys. Rev. D **92**, 123009 (2015), arXiv:1504.03291 [astro-ph.CO].
- [80] M. Hindmarsh, Phys. Rev. Lett. **120**, 071301 (2018), arXiv:1608.04735 [astro-ph.CO].
- [81] M. Hindmarsh, S. J. Huber, K. Rummukainen, and D. J. Weir, Phys. Rev. D **96**, 103520 (2017), [Erratum: Phys. Rev. D 101, 089902 (2020)], arXiv:1704.05871 [astro-ph.CO].
- [82] J. Ellis, M. Lewicki, and J. M. No, JCAP **04**, 003 (2019), arXiv:1809.08242 [hep-ph].
- [83] M. Hindmarsh and M. Hijazi, JCAP **1912**, 062 (2019), arXiv:1909.10040 [astro-ph.CO].
- [84] J. Ellis, M. Lewicki, and J. M. No, JCAP **07**, 050 (2020), arXiv:2003.07360 [hep-ph].
- [85] J. Ellis, M. Lewicki, and V. Vaskonen, JCAP **11**, 020 (2020), arXiv:2007.15586 [astro-ph.CO].
- [86] H. L. Child and J. Giblin, John T., JCAP **10**, 001 (2012), arXiv:1207.6408 [astro-ph.CO].
- [87] S. J. Huber and T. Konstandin, JCAP **09**, 022 (2008), arXiv:0806.1828 [hep-ph].
- [88] D. J. Weir, Phys. Rev. D **93**, 124037 (2016), arXiv:1604.08429 [astro-ph.CO].
- [89] R. Jinno and M. Takimoto, Phys. Rev. D **95**, 024009 (2017), arXiv:1605.01403 [astro-ph.CO].
- [90] R. Jinno and M. Takimoto, JCAP **01**, 060 (2019), arXiv:1707.03111 [hep-ph].
- [91] T. Konstandin, JCAP **03**, 047 (2018), arXiv:1712.06869 [astro-ph.CO].
- [92] R. Jinno, H. Seong, M. Takimoto, and C. M. Um, JCAP **1910**, 033 (2019), arXiv:1905.00899 [astro-ph.CO].
- [93] R. Jinno, T. Konstandin, and H. Rubira, (2020), arXiv:2010.00971 [astro-ph.CO].
- [94] L. Randall and G. Servant, JHEP **05**, 054 (2007), arXiv:hep-ph/0607158 [hep-ph].
- [95] T. Konstandin and G. Servant, JCAP **1112**, 009 (2011), arXiv:1104.4791 [hep-ph].
- [96] T. Konstandin and G. Servant, JCAP **07**, 024 (2011), arXiv:1104.4793 [hep-ph].
- [97] B. von Harling and G. Servant, JHEP **01**, 159 (2018), arXiv:1711.11554 [hep-ph].
- [98] A. Kobakhidze, C. Lagger, A. Manning, and J. Yue, Eur. Phys. J. C **77**, 570 (2017), arXiv:1703.06552 [hep-ph].
- [99] T. Hambye, A. Strumia, and D. Teresi, JHEP **08**, 188 (2018), arXiv:1805.01473 [hep-ph].
- [100] M. Aoki and J. Kubo, JCAP **04**, 001 (2020), arXiv:1910.05025 [hep-ph].
- [101] K. Fujikura, Y. Nakai, and M. Yamada, JHEP **02**, 111 (2020), arXiv:1910.07546 [hep-ph].
- [102] X. Wang, F. P. Huang, and X. Zhang, JCAP **05**, 045 (2020), arXiv:2003.08892 [hep-ph].
- [103] S. R. Coleman and E. J. Weinberg, Phys. Rev. D **7**, 1888 (1973).
- [104] K. Saikawa and S. Shirai, JCAP **05**, 035 (2018), arXiv:1803.01038 [hep-ph].
- [105] S. W. Hawking, I. G. Moss, and J. M. Stewart, Phys. Rev. **D26**, 2681 (1982).
- [106] S. Weinberg, *Gravitation and Cosmology* (John Wiley and Sons, New York, 1972).